CrossMark

Pore Network Modeling of Shale Gas Reservoirs: Gas Desorption and Slip Flow Effects

Jalal Foroozesh[1] [iD] · **Amr Ibrahim Mohamed Abdalla[1]** · **Zhien Zhang[2]**

Abstract

Shale reservoirs are characterized by very low permeability in the scale of nano-Darcy. This is due to the nanometer scale of pores and throats in shale reservoirs, which causes a difference in flow behavior from conventional reservoirs. Slip flow is considered to be one of the main flow regimes affecting the flow behavior in shale gas reservoirs and has been widely studied in the literature. However, the important mechanism of gas desorption or adsorption that happens in shale reservoirs has not been investigated thoroughly in the literature. This paper aims to study slip flow together with gas desorption in shale gas reservoirs using pore network modeling. To do so, the compressible Stokes equation with proper boundary conditions was applied to model gas flow in a pore network that properly represents the pore size distribution of typical shale reservoirs. A pore network model was created using the digitized image of a thin section of a Berea sandstone and scaled down to represent the pore size range of shale reservoirs. Based on the size of pores in the network and the pore pressure applied, the Knudsen number which controls the flow regimes was within the slip flow regime range. Compressible Stokes equation with proper boundary conditions at the pore's walls was applied to model the gas flow. The desorption mechanism was also included through a boundary condition by deriving a velocity term using Langmuir-type isotherm. It was observed that when the slip flow was activated together with desorption in the model, their contributions were not summative. That, is the slippage effect limited the desorption mechanism through a reduction of pressure drop. Eagle Ford and Barnett shale samples were investigated in this study when the measured adsorption isotherm data from the literature were used. Barnett sample showed larger contribution of gas desorption toward gas recovery as compared to Eagle Ford sample. This paper has produced a pore network model to further understand the gas desorption and the slip flow effects in recovery of shale gas reservoirs.

Keywords Shale gas reservoirs · Pore network modeling · Stokes flow · Gas desorption · Slip flow

✉ Jalal Foroozesh
  jalal.foroozesh@gmail.com; jalal.foroozesh@utp.edu.my

[1] Petroleum Engineering Department, Universiti Teknologi PETRONAS, Perak, Malaysia

[2] School of Chemistry and Chemical Engineering, Chongqing University of Technology, Chongqing 400054, China

🗌 Springer

List of symbols

N	Coordination normal to the wall
L_s	Slip length (m)
u_T	Thermal motion velocity
u_s	Slip velocity (m/s)
u_w	Wall velocity (m/s)
u_d	Velocity term for desorption boundary condition
C_1	First-order slip coefficient
u	Fluid velocity
K	Permeability (m^2)
M	Gas molecular mass (kg/mol)
L	Length (m)
p	Pore pressure (Pa)
D	Diffusion coefficient
D_n	Knudsen diffusion coefficient
d_p	Pore diameter
A	Cross-sectional area (m^2)
T	Temperature (K)
vl	Langmuir volume (m^3/kg)
$R = 8.31445 \times 10^3$	Gas constant ($g/m^2/s^2/mol/K$)

Greek Letters

λ	Mean free path of flowing gas
μ	Gas viscosity (Pa s)
σ_v	Tangential accommodation coefficient
ρ	Gas density (kg/m^3)
ρ_r	Rock density (kg/m^3)

Subscript

s Slip

Abbreviations

K_n Knudsen number
Re Reynold number

1 Introduction

There has been a recognizable increase in the production and development of shale gas reservoirs in the recent years. Incited by the presence of enormous reserves and having lower CO_2 emissions, shale gas has garnered more and more attention (Sutton et al. 2010). Shale gas

exists within shale reservoirs in three forms: free gas within pores and micro-cracks, adsorbed gas on the surface of organic and inorganic matter and dissolved gas in water (Strapoc et al. 2010). In shale gas reservoirs, apart from a small amount of gas which is dissolved in the formation water, the free gas is stored in pores and cracks, whereas the adsorbed gas is stored on the surface of shale particles and organic matter (Wang et al. 2016). Free gas and adsorbed gas constitute the largest proportion of present gas in shale reservoirs, where adsorbed gas marks 20% to 85% of initial-gas-in-place in several shale gas reservoirs in US shale basins (Curtis 2002). The permeability of rock matrix in shale reservoirs, unlike conventional rock types, is no longer an inherent rock property but is also dependent on gas pressure and temperature (Civan 2010; Darabi et al. 2012; Moghaddam et al. 2015). The flow within shale reservoirs is divided into several regimes that are characterized or classified using what is known as Knudsen number. The reason for the existence of these various flow regimes can be traced back to the basic theory of gas diffusion for further understanding. The main concept of this theory is based on the gas diffusion from an area of higher concentration to an area of lower concentration, and the magnitude of the diffusive flux produced is the product of the concentration gradient multiplied by a diffusion coefficient (Liu et al. 2018). Based on classic statistical physics, the diffusion coefficient can be estimated as a function of mean free path (λ) shown below (Singh and Javadpour 2013):

$$D = \frac{1}{3}\lambda u_{\mathrm{T}}, \tag{1}$$

where D is the diffusion coefficient, u_{T} is the averaged magnitude of thermal motion speed and λ is the mean free path for molecules shown in Eq. 2. The high temperature and pressure conditions that usually govern shale reservoirs have an effect on gas PVT properties, and hence taking real gas properties into consideration should provide more realistic results. The mean free path for real gases can be estimated through the equation shown below (Villazon et al. 2011):

$$\lambda = \sqrt{\frac{\pi Z R T}{2M}} \frac{\mu}{p} \tag{2}$$

The mean free path represents the area within which gas molecules move. When the pore diameter of said porous media is smaller than the estimated mean free path, the flow of gas molecules is constricted to the smaller area established by the pore diameter. Hence, the diffusion coefficient (Eq. 1) is altered to include the actual pore diameter as follows (Singh and Javadpour 2013):

$$D_n = \frac{1}{3}d_{\mathrm{p}}u, \tag{3}$$

where d_{p} is the pore diameter and D_n is referred to as Knudsen diffusion coefficient.

Figure 1 shows the two scenarios mentioned above where in the first case (a) the mean free path is smaller than pore diameter and hence normal gas diffusion occurs, whereas in case (b) the pore diameter is smaller than the mean free path causing an increased interaction with the solid walls. This is called Knudsen diffusion which leads to the development of the various flow regimes (Sun et al. 2017).

The dimensionless Knudsen number (K_n) which is a ratio of mean free path to pore diameter is used to classify the different flow regimes as shown in Table 1:

$$K_n = \frac{\lambda}{d_{\mathrm{p}}}, \tag{4}$$

where λ is the mean free path and d_{p} is pore diameter.
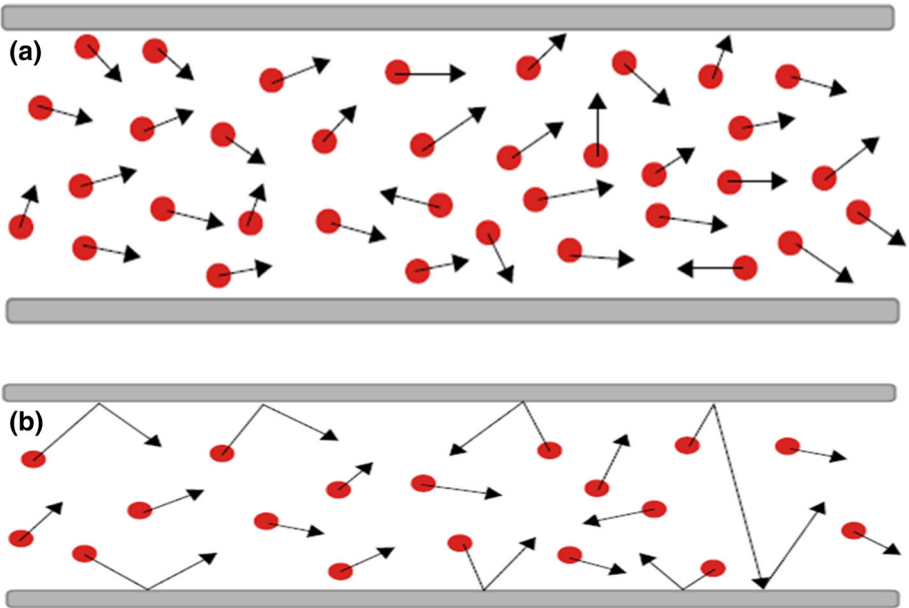
Fig. 1 Schematic of the movement of gas molecules: **a** normal gas diffusion and **b** Knudsen diffusion (Liu et al. 2018)

Table 1 Different flow regimes at different Knudsen numbers (Song et al. 2017)

Knudsen number (K_n)	Flow regime
0 to 10^{-3}	Continuum flow
10^{-3} to 10^{-1}	Slip flow
10^{-1} to 10^{1}	Transition flow
10^{1} to ∞	Free molecular flow

Depending on the value of Knudsen number, different flow regimes that is summarized in Table 1 can be experienced during fluid flow in shale gas reservoirs:

- *Continuum Flow* describes a minimal molecular interaction with pore walls. The diffusion is mainly mechanized through molecule to molecule collisions. The pore diameter is much larger than the mean free path resulting in Knudsen numbers lower than 10^{-3}. Continuum equations such as Darcy's equation or Navier–Stokes (NS) equation can be adequately used to model continuum flow.
- *Slip Flow* occurs when the gas velocity at pore surface is not zero. This is due to the increased interaction of gas molecules with pore walls as a result of the smaller pore diameters (Li et al. 2017). Slip velocity was first introduced by Navier (Zhang et al. 2012a), where through his model, it was shown that slip velocity shares a proportional relationship with the shear rate of the flow at pore walls. The Knudsen number in this regime lies between 10^{-3} and 10^{-1}. However, some references have reported this to be between 10^{-2} and 10^{-1} (Moghaddam and Jamiolahmady 2016; Ahmadi and Shadizadeh 2015). The effects induced by pore wall interactions are, however, limited to what is known as the Knudsen layer, where gas–solid interactions are dominant (Fig. 2). In other words, beyond
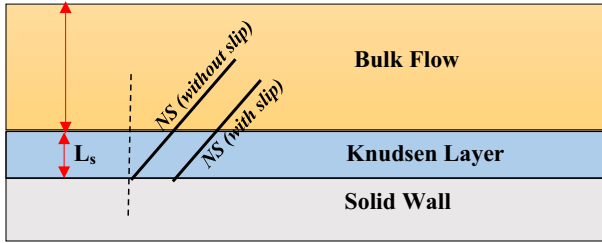
Fig. 2 Schematic presentation of Knudsen layer during gas flow

the Knudsen layer, gas flow can still be studied within the context of fluid mechanics. Hence, by introducing a slip boundary condition at the pore surface, the effect of the slip within the Knudsen layer can be accounted for (Karniadakis et al. 2006).

- *Transitional flow*, is a combination of slip flow and Knudsen flow (Knudsen diffusion); hence, a general model can be established using the sum weighted average of slip flow and Knudsen flow mechanisms. The Knudsen range falls between 10^{-1} and 10^{1}.
- *Molecular-free flow* is a flow regime which is completely dominated by gas–solid interaction. That is, the intermolecular collision is not important. Molecular dynamics (Gad-el-Hak 1999) or the Lattice Boltzmann method (Shabro et al. 2012) can be used to study this regime. This regime has Knudsen numbers values higher than or equal to 10^{1}.

As described above, several different parameters come into the characterization of shale reservoirs, ranging from the different flow regimes to other physical phenomena such as adsorption and poroelastic stress effects; all attribute contributions to the final output specifically in terms of apparent absolute permeability (Moghaddam et al. 2015; Moghaddam and Foroozesh 2017). In terms of adsorption, the adsorbed layer of methane which is a characteristic of shale reservoirs constitutes a large amount of the gas mass flux that is produced. There is a considerable amount of adsorbed methane occupying kerogen pore surfaces which can be driven by chemical potential gradient in the shape of surface diffusion, instilling another mechanism that contributes to transport in shale along with slip flow and Knudsen diffusion (Fathi and Akkutlu 2009; Freeman et al. 2011; Kang et al. 2011; Sheng et al. 2014; Sondergeld et al. 2010; Wu et al. 2015). All the mechanisms mentioned above can be considered as non-Darcy flow corrections and be lumped and reported in the form of apparent permeability of shale reservoirs. Table 2 shows a summary of apparent permeability models from previous studies which include different non-Darcy flow corrections. These corrections include corrections for the Knudsen diffusion, slip flow and surface diffusion (adsorption). The complexity incited by pore structures and the unique storage ability of shale rock induce gas flow complexities within shales (Lin et al. 2017), influenced strongly by adsorption and diffusion (Moridis et al. 2010). Thus, an understanding of methane diffusion and adsorption in low-permeability shale reservoirs is crucial for formation evaluation (Wu et al. 2015). In the area of surface diffusion (adsorption), some research has been done; however, its effects and contribution to shale gas flow are further to be understood.

Surface diffusion and bulk gas diffusion were incorporated in a study done by Fathi and Akkutlu (2009) and (2012) where it was described that surface diffusion exists as an intrinsic property of gas release associated with low-permeability reservoirs. A measurement of surface diffusivity conducted on kerogen pore surface through isothermal pulse-decay testing produced results in the range of 1.55×10^{-7} to 8.80×10^{-6} m²/s (Kang et al. 2011). The

Table 2 Summary of apparent permeability models

Model	Description
Javadpour (2009)	Considers first-order slip flow and Knudsen diffusion
Darabi et al. (2012)	Considers impact of surface roughness using Javadpour's model
Sheng et al. (2015)	Considers first-order slip flow as well as Knudsen diffusion while taking into account surface diffusion effects
Pang et al. (2017)	Considers second-order slip flow and surface diffusion, with consideration of the density profile using SLD-PR model
Moghadam and Chalaturnyk (2014)	Considers Klinkenberg slip theory in a quadratic format
Fink et al. (2017)	Considers fluid dynamics together with poroelastic effect

consideration of methane adsorption as monolayer adsorption and using Langmuir equation, Langmuir–Freundlich (L–F) equation and modified Langmuir (M–L) equation has been successfully applied for the evaluation of methane adsorption in several studies (Ahmadi and Shadizadeh 2015; Etminan et al. 2014; Yang et al. 2015). The Langmuir theorem has an underlying assumption which states that only one layer of adsorbed gas covers the surface of shale rock.

Recently, pore scale study of shale reservoirs using pore network modeling, has furthered our understanding of the physical mechanisms behind gas production from shale (Javadpour 2009). It has provided a cost-effective method to produce accurate predictions on local transport phenomena where it links microscale description of medium to macroscopic fluid characteristics such as porosity and permeability (Mehmani et al. 2013). In addition, its flexibility allows for variations in system parameters for further analysis. Pore scale models were initially developed by Fatt (1956) where he simulated the capillary pressure curve as a function of saturation using pore network models (Fatt 1956). Following that, pore network models were further enhanced and adapted to several fields including reservoir engineering, where it opened up new gateways in understanding constituting relationships of two-phase flow and further down the road expanding into the exploration of transport phenomena within porous media. Several studies used pore network modeling to explore the effects of various phenomena that exist in shale reservoirs, for example, the contribution of slip flow and Knudsen diffusion has been coupled in several models (Darabi et al. 2012; Javadpour 2009; Liu et al. 2018) with the main focus in these studies being fluid flow dynamics within the set regimes in shale reservoirs. Other works included coupled effects of slip flow, compressibility and sorption such as a study conducted by Huang et al. (2015); however, the main focus on the sorption term in many papers is the quantification of adsorption and not many studies are conducted to estimate the contribution of the desorption term to shale permeability. Development of a representative network model is very important, and key factors of pore size distribution, pore throat diameters as well as interconnectivity within the porous media should be carefully established. In other words, although the pores and throats are to be described through relatively simpler geometrical shapes, the models should preserve the realistic microscale properties, mainly pore and throat size distribution (Mehmani et al.

2013). In pore network modeling, reservoir (porous media) is considered as a collection of pores where Hagen–Poiseuille equation is commonly applied as a simplified form of continuum flow of Navier–Stokes equation. The results of these pore flow studies are used to discover the flow mechanisms or to obtain pertinent parameters of the porous media.

The Navier–Stokes equation is a reliable method to describe the motion of fluids within the continuum assumption. However, this flow equation is also a function of Reynold number (*Re*) which is the ratio of inertial forces to viscous forces as shown in Eq. 5:

$$Re = \frac{\rho u L}{\mu} \tag{5}$$

In the case of low Reynold numbers which occurs when the fluid velocity (u) is very low, viscosity (μ) very high or the length scale (L) of the flow very small (nanoscale), a linearization of the Navier–Stokes equations known as Stokes flow named after George Gabriel Stokes is used to model the flow, where in Stokes flow, the inertial forces are assumed to be negligible (Kim and Karrila 2013).

In this paper, a dynamic pore-network flow model is created to allow for a more accurate quantification of slip and desorption effects on shale gas flow. Our model focuses on investigating the contribution of slip and desorption effects in terms of velocity enhancement which is then expressed in terms of apparent permeability. In this study, the commonly used Hagen–Poiseuille equation which mainly describes incompressible flow in steady state is replaced by the transient Stokes equation for compressible fluid. Therefore, more accurate and reliable results are expected. Serving as a reliable dynamic flow equation, the Stokes equation is coupled with a slip boundary condition. Desorption mechanism is also considered by adapting a boundary condition through a velocity term derived using Langmuir-type isotherm equation. Some new results showing the flow behavior under slip with desorption mechanisms are presented. The permeability enhancement under varying pore pressures is quantified. The main focus of this study is slip and desorption effects; hence, the model is run within the slip flow regime. The effective stress which may influence the flow behavior in shale gas reservoirs was excluded in this study.

2 Methodology

Shale gas reservoirs have been characterized by tiny and complicated pores, having nanopores with diameters in the range of 1–200 nm (Cipolla et al. 2009). According to the nuclear magnetic resonance, scanning electron microscope and high-pressure mercury measurement techniques, the main pore sizes are approximated to be around 5–20 nm (Sakhaee-Pour and Bryant 2012). The average diameter for the connecting pore throats ranges between 1 and 10 nm. A typical pore network is constructed of two basic elements, pores and pore throats, and due to the smaller pore throat diameter, the main resistance to flow within the system will be associated with pore throat diameter (Huang et al. 2016). To study the flow mechanism in shale reservoirs at pore scale, an image of a thin slice of a Berea sandstone presented in the literature (Keller et al. 1997) was used to make a pore network model as shown in Fig. 3. The image was taken using an optical microscope and then digitized by Hornbrook et al. (1991).

To improve the connectivity in the two-dimensional micromodel, the digitized image was modified slightly by Keller et al. (1997). The pore network is scaled down in this study from its original size (microscale) to nanoscale range to represent the typical pore sizes in shale reservoirs. Based on the size of the pores and the pore pressures applied in this study, the Knudsen number values fall within the range of continuum to slip flow as shown in Fig. 4.
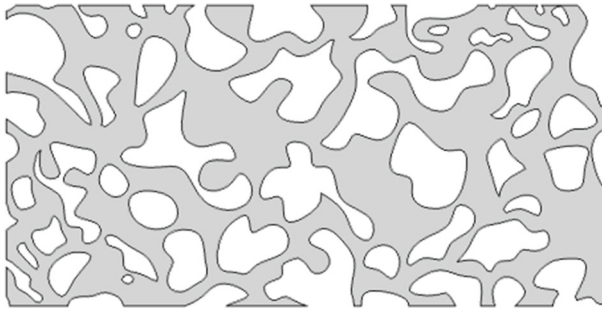
Fig. 3 Pore network structure, the white areas are the grains and the gray areas are the pores and throats (Keller et al. 1997). The model extends 705 nm in the *x* direction and 352 nm in the *y* direction; pore diameters range in size from 5 to 20 nm
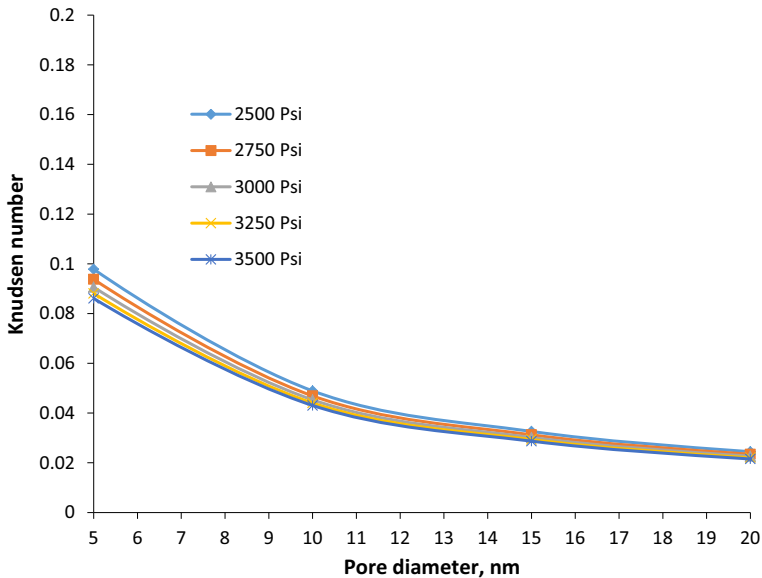
Fig. 4 Estimation of Knudsen number for different pressures at different pore diameters embedded in the network for real gas

The aim was to ensure the system remains within the slip flow regime to exclude the Knudsen diffusion flow and to maintain the validity of Stokes flow as well.

The subsequent assumptions were made during the modeling process:

1. The pores are occupied by methane which is a compressible fluid with variable density and viscosity.
2. The model is run under a constant temperature.
3. No stress effects.
4. No gravity effect (horizontal system).

As mentioned earlier, the flow within the shale reservoirs is divided between several regimes at any given time and the dominance of said regimes is governed by the geometrical aspects of the reservoir as well as reservoir temperature and pressure. However, in this study

only the viscous flow with slip boundary condition together with desorption mechanism is considered.

2.1 Viscous Flow

Beyond the established Knudsen layer that is governed by fluid–solid interactions, the viscous flow can be modeled using continuum equations. The Navier–Stokes equation is adopted to describe the viscous compressible Newtonian fluid flow as methane gas in shale reservoirs is a compressible fluid (Batchelor 2000):

$$\rho\left(\frac{d\vec{u}}{dt} + \vec{u} \cdot \nabla \vec{u}\right) = -\nabla p + \mu\nabla^2\vec{u} + \frac{1}{3}\mu\nabla(\nabla \cdot u), \tag{6}$$

where ρ is the fluid density in kg/m^3; $\vec{u}$ is the velocity field; and μ is the gas viscosity, Pa s.

Due to the small length scale of our system, the inertial term in the Navier–Stokes equation is negligible; hence, the equation is reduced to the Stokes equation by ignoring the inertial term as shown below (Kim and Karrila 2013):

$$\rho\left(\frac{d\vec{u}}{dt}\right) = -\nabla p + \mu\nabla^2\vec{u} + \frac{1}{3}\mu\nabla(\nabla \cdot u) \tag{7}$$

The density and viscosity of gas (methane) change with pressure in the above equation. To calculate them, the following equations were obtained by fitting process using the values taken from NIST Chemistry Webbook (NIST 2018) within the pressure range of 1–35 MPa at fixed temperature of 40 °C:

$$\rho = -3 \times 10^{-21}p^3 + 8 \times 10^{-14}p^2 + 7 \times 10^{-6}p - 1.8655, \tag{8}$$

$$\mu = -3 \times 10^{-28}p^3 + 2 \times 10^{-20}p^2 + 6 \times 10^{-14}p + 1 \times 10^{-5}, \tag{9}$$

where p is pressure in Pa.

2.2 Slip Flow

Based on the physics of slip flow, the slip velocity is defined through the following equation (Moghaddam and Jamiolahmady 2016; Moghaddam et al. 2015):

$$u_s = L_s\left(\frac{\partial u}{\partial n}\right)_s, \tag{10}$$

where u_s is slip velocity, L_s is the slip length and n is the coordinate normal to the wall. Moreover, the slip velocity can also be translated as follows:

$$u_s - u_w = C_1\lambda\left(\frac{\partial u}{\partial n}\right)_s, \tag{11}$$

where C_1 is the slip coefficient that in turn is dependent on the tangential momentum accommodation coefficient (σ_v) and expressed as follows:

$$C_1 = \alpha_s\frac{2 - \sigma_v}{\sigma_v} \tag{12}$$

α_s is a constant which is unity in the Maxwell model (Zhang et al. 2012b). u_w is the velocity at the surface when there is no slip which is zero here. λ is the mean free path for methane molecules that is calculated using Eq. 2 and is a function of pressure. A typical value of 0.9 is used for σ_v parameter here (Karniadakis et al. 2006).

2.3 Desorption

In order to describe the effect of desorption behavior within the shale porous media, the widely used Langmuir theorem was applied. The Langmuir equation can be written in the following form (Langmuir 1916):

$$v' = \frac{p \times vl}{p + pl},$$

(13)

where v' is volume of adsorbed gas; p is the pore pressure; vl is Langmuir volume; and pl is Langmuir pressure. vl is the maximum gas that can be adsorbed at large pressures, and pl is the pressure at which the amount of gas adsorbed is half of the maximum adsorbed gas (vl). Usually, the vl is reported in volume per weight (volume/weight) unit and as a result, v' has also a volume/weight unit. Therefore, the following formulation is used to convert it into volume unit:

$$v = \frac{p \times vl}{p + pl} \times \rho_r \times h \times A,$$

(14)

where v is gas content from the measured isotherm in m^3, vl is the Langmuir adsorbed gas in m^3/Kg, ρ_r is the density of rock in kg/m^3, A is the wall (grain) surface area in m^2 and h is the wall (grain) thickness in m. An adaptation of the Langmuir equation was instilled as a boundary condition in our system where it is described as a velocity term (fixed velocity boundary condition) added due to the desorption of methane from pore walls (Fig. 5) through the following mass balance equation:

$$\dot{m}_{in} - \dot{m}_{out} = \frac{dm}{dt}$$

(15a)

If our system is the rock part:

$$-\dot{m}_{out} = \frac{dm}{dt},$$

(15b)

$$-\rho u_d A = \frac{d(\rho v)}{dt},$$

(15c)

where ρ is the density of gas which is a function of pressure, u_d is the velocity of desorbed gas leaving the rock and A is the rock surface area in front of the flow. v is the gas content of the rock presented in Eq. 14 which is a function of pressure. Further mathematical manipulations will result in the following equations:

$$u_d = -\frac{1}{\rho A} \frac{d(\rho v)}{dt} = -\frac{1}{\rho A} \frac{d(\rho v)}{dp} \frac{dp}{dt} = -\frac{vl \times \rho_r \times h \times A}{\rho A} \frac{d\left(\rho \frac{p}{p+pl}\right)}{dp} \frac{dp}{dt}$$

(16a)

$$u_d = -\frac{vl \times \rho_r \times h}{\rho} \left[\rho \frac{d\left(\frac{p}{p+pl}\right)}{dp} + \frac{p}{p+pl} \frac{d\rho}{dp}\right] \frac{dp}{dt}$$

(16b)

Fig. 5 Desorption process

Pore (gas)

Rock (solid + desorbed gas)
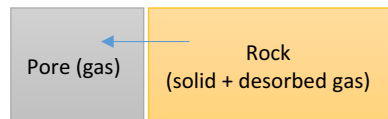
Equation 16b shows the velocity of gas desorbed from the wall surface (solid) entering the pores. It is used as a velocity boundary condition to capture the desorption effect. To calculate the $\frac{d\rho}{dt}$ term in Eq. 16b, the gas density equation presented in Eq. 8 is used. The thickness was taken as the grain size of grains surrounding the pores, which was taken as 4 microns, the maximum for clay grain sizes (Crain 2002). Density of shale rocks ranges between 2.2 and 2.6 g/cc (Crain 2002), so an average value of 2.4 g/cc was taken as the density.

Barnett shale and Eagle Ford shale samples were investigated here. The Langmuir parameters (vl and pl) for the mentioned samples were attained from Langmuir isotherms measured by Heller and Zoback (2014) at 40 °C as shown in Fig. 6a, b.

Langmuir volume and pressure are extracted from Fig. 6a, b and shown in Table 3.

A finite element package was used to solve the above equations in an unsteady state condition. That is, the compressible Stokes flow equation with slip boundary condition (no zero velocity) on wall surface was solved numerically when a velocity boundary condition
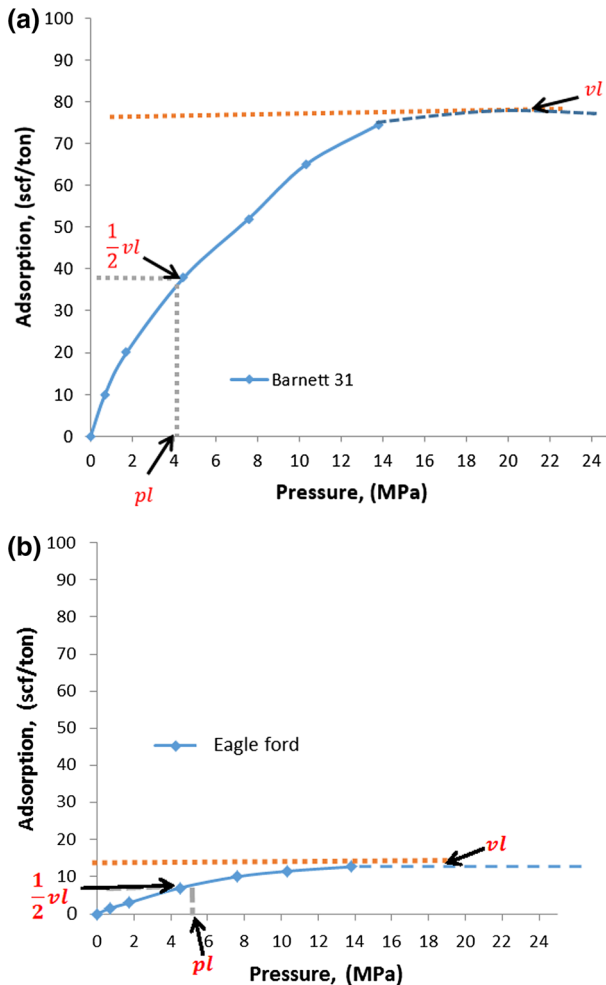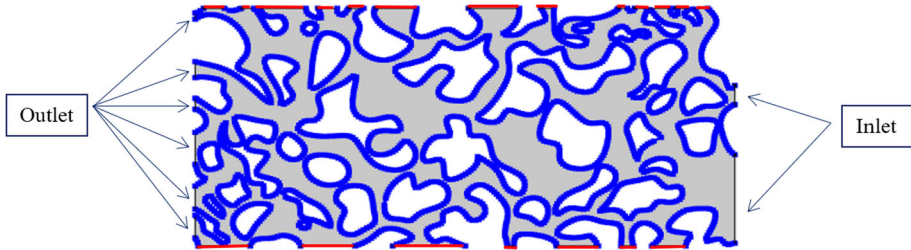

Fig. 6 Adsorption versus pore pressure for **a** a Barnett shale sample. **b** Eagle Ford shale sample

Table 3 Langmuir volume and pressure of Barnett and Eagle Ford shale samples (Heller and Zoback 2014)

	Barnett 31	Eagle Ford 127
pl (MPa)	4.0	4.8
vl (scf/ton)	74.4	12.7

Fig. 7 Pore network model. The pressure gradient is set at 2 MPa/m (1.4 Pa/nm); the simulation is run at a time step size of 0.1 s for 2 s

is assigned to the wall through a velocity term derived above (Eq. 16b) to consider the desorption mechanism. A constant pressure at inlet and outlet of the network was assigned so that a differential pressure (pressure drop) of 2 MPa/m was applied to our model as shown in Fig. 7. In Fig. 7, inlet and outlet boundaries are shown at the right and left sides, respectively. The top and bottom boundaries are shown by red lines assigned to have a symmetry boundary condition, whereas the blue lines are pore walls where the slip boundary condition and or desorption is applied. The system pressure was set so that pore pressure would range from 2500 Psi up to 3500 Psi. This pressure range was set based on typical shale reservoir pressures reported in the literature (Crain 2002).

The slip and desorption boundary conditions were combined through the following velocity term:

$$u_{s+d} = u_s + u_d = C_1 \lambda \left(\frac{\partial u}{\partial n}\right)_s + \left(-\frac{vl \times \rho_r \times h}{\rho}\left[\rho\frac{d\left(\frac{p}{p+pl}\right)}{dp} + \frac{p}{p+pl}\frac{d\rho}{dp}\right]\frac{dp}{dt}\right) \quad (17)$$

2.4 Permeability

Finally, the permeability for the whole pore network can be calculated using Darcy's equation as follows:

$$K = \frac{V \times \Delta x \times \mu}{\Delta p}, \quad (18)$$

where K is permeability in Darcy, V is average velocity within the network in cm/s, Δx is length in x direction in cm, μ is viscosity in cp and Δp is ($p_{inlet} - p_{outlet}$) in atm.

3 Results and Discussion

3.1 Slip Flow

An initial run was primarily conducted without the consideration of the induced desorption or slip flow effect as a reference to the expected change in velocity profile. Later on, only slip boundary condition was applied. Figure 8 shows a comparison of permeability profiles developed by modeling gas flow using the Stokes equation with and without the application of the slip flow boundary condition at different pore pressures.

It is clearly seen that without the slip boundary condition, much of the actual mobility of the flowing gas is not accounted for. As can be noticed from Fig. 8, almost a linear permeability profile with pore pressure is developed once gas slippage effect is taken into consideration. It should be noted that the portrayed profile is in accordance with the first-order slip assumption as no deviations from the linear relationship occur. It is also worth mentioning that due to our relatively large pore throat diameter, the Knudsen numbers for the pressure range used all fall within the slip regime; hence, the permeability increase is almost consistent; however, beyond the slip flow regime slip effect, a linear profile may no longer be produced. The effects of slip flow are slightly subdued at higher pressures as the higher pressure term works to limit the mean free path of the gas molecules. In other words, at high pressures we can notice a lower increase in permeability, but as pressure decreases, this allows the mean free path for the gas molecules to expand allowing the slip flow term to have a more dominant effect on gas flow leading to a larger apparent permeability. Figure 9 shows the velocity profile within the pore network. It can be observed that the velocity is noticeably higher at smaller pore throats within the network. Moreover, due to tortuosity and heterogeneity of the network, the fluid is preferentially flowing through some specific routes while the velocity is zero at dead-end pores.
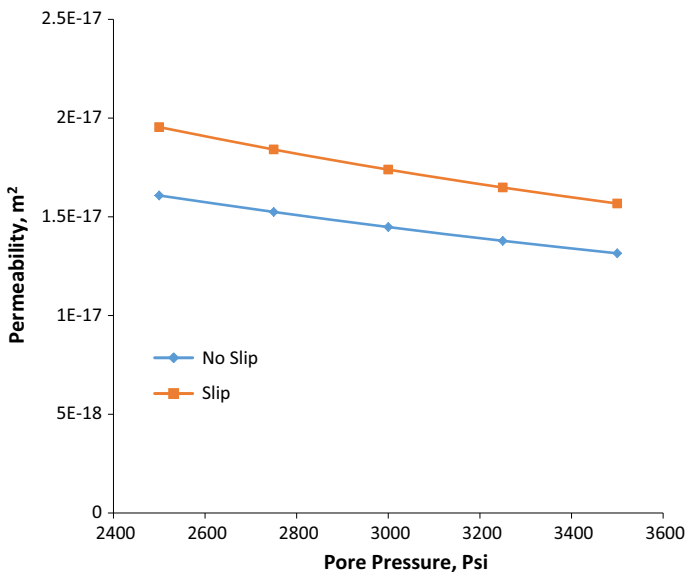

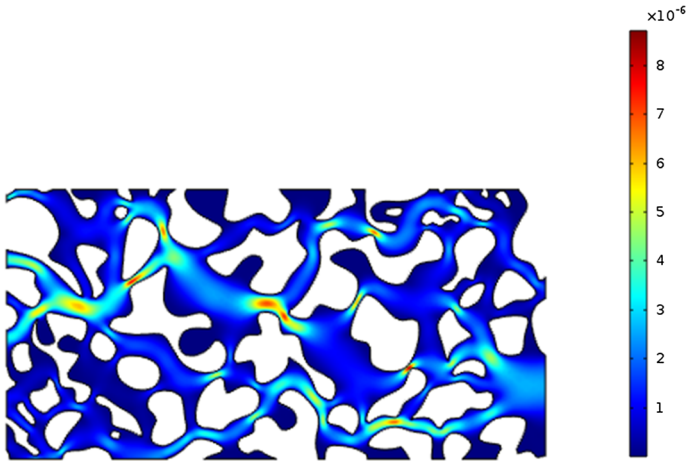**Fig. 8** Permeability profile with and without slip effect versus pore pressure
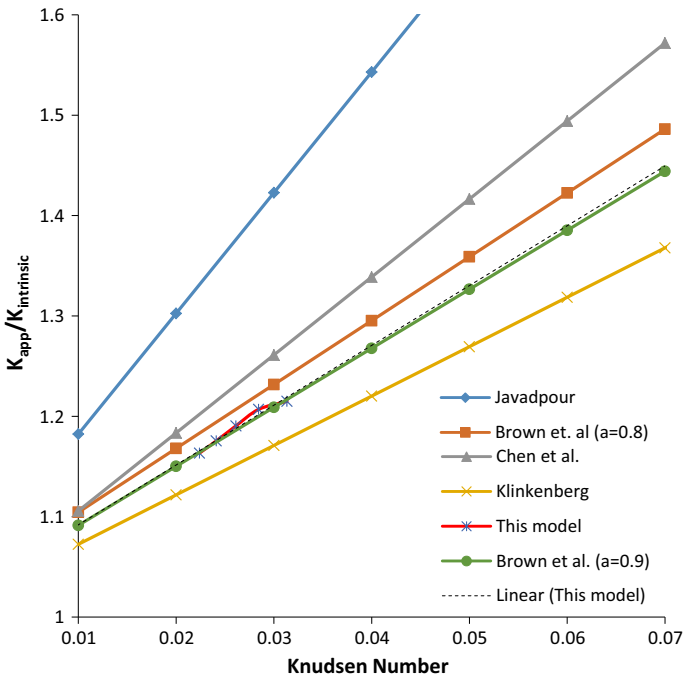
Fig. 9 Velocity profile (unit: m/s)

Fig. 10 Comparison between different models based on permeability enhancement

The enhancement in permeability was compared to that of other models found in the literature to validate the accuracy of the given model. This is shown in Fig. 10 where the ratio of apparent permeability (with slippage effect) to intrinsic permeability (without slippage effect) versus pore pressure is given.

As can be seen in Fig. 10, for Knudsen numbers between 0.01 and 0.07 which is within slip flow regime range, our model shows a reasonable fit with Brown et al. (1946) model where

they have considered a tangential accommodation coefficient of 0.9 to take into consideration wall surface roughness. It should be noted that, in Fig. 10, 'Linear (this model)' curve is obtained by extrapolating the results of our model while 'This model' curve is calculated directly by our model. The results of Javadpour's model presented in Fig. 10 are different probably because he considers both slip flow and Knudsen diffusion flow regimes while using Hagen–Poiseuille non-compressible flow equation. Moreover, our results are different from the Chen et al.'s results (2015) as they used the dusty gas model to investigate the permeability behavior. Furthermore, our results are different from those by Klinkenberg's model (1941) considering he used an empirical equation to study the slip flow effect.

3.2 Desorption Together with Slip Flow

The desorption phenomenon which is another occurrence within shale porous media was taken into consideration in this paper as well. The desorption was included through a velocity boundary condition derived above (Eq. 16b). The permeability enhancement induced by the desorption, slip and desorption together with slip is shown in Fig. 11 for Eagle Ford shale sample.

It is worth mentioning that the percentage of permeability enhancement ($K_{enhancement}$) is calculated by finding the difference between the apparent permeability obtained from the model with including slip or desorption or slip together with desorption mechanisms (K_{app}) and the intrinsic permeability obtained from the model without any slip and desorption mechanism ($K_{intrinsic}$) and then dividing it by intrinsic permeability as shown below:

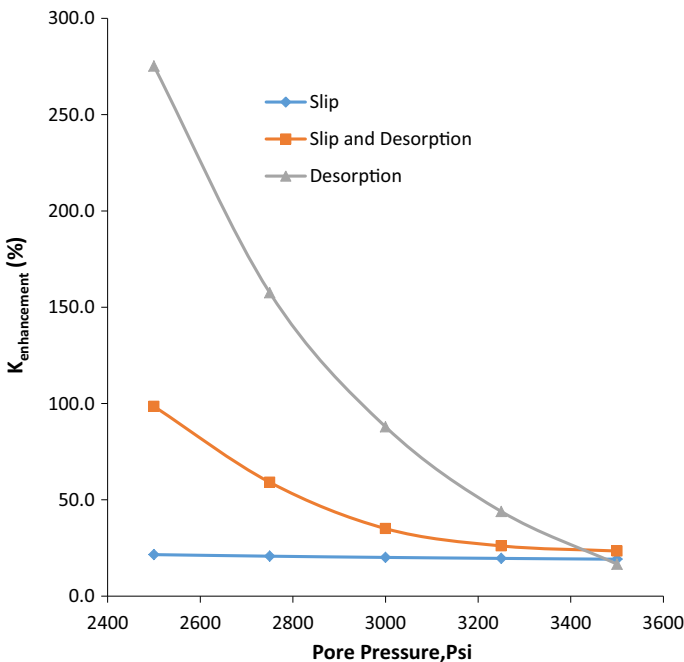$$K_{enhancement} = \frac{K_{app} - K_{intrinsic}}{K_{intrinsic}} \times 100 \tag{19}$$

Fig. 11 Permeability versus pore pressure

Table 4 Contribution of slip flow, desorption and slip together with desorption to permeability for Eagle Ford sample

Pore pressure (Psi)	Permeability enhancement by slip flow (%)	Permeability enhancement by desorption (%)	Permeability enhancement by slip flow and desorption (%)
2500	21.5	275.2	98.5
2750	20.7	157.6	59.1
3000	20.1	87.9	35.1
3250	19.6	43.9	26.1
3500	19.2	16.6	23.4

The $K_{\text{enhancement}}$ values presented in Fig. 11 for different mechanisms are summarized in Table 4.

We can see that as pressure falls, the slippage effect increases slightly. The individual contribution of slip is approximately 19.2% at 3500 Psi and continues to increase up to 21.5% at 2500 Psi. It is well known that gases at high pressures show less slip flow effect as at higher pressures, their behavior becomes more liquid-like. In other words, at lower pressures, slip contribution is expected to be higher. This trend has been discussed in the literature as the Klinkenberg effect (Klinkenberg 1941). Table 4 also shows the enhancement of permeability due to desorption. It can be seen that as a contribution of individual desorption, the permeability of the system is appreciably increased and the desorption contribution is 16.6% at 3500 Psi and has increased to 275.2% at 2500 Psi. Considering the physics of the desorption and considering the Langmuir isotherm curves presented above, the driving force for gas desorption is the pressure difference between pore pressure and pressure at which the maximum amount of gas (vl) is adsorbed which becomes larger at lower pore pressures; hence, at lower pore pressures, a higher contribution due to gas desorption is noticed. Given the nature of shale matrix, the portion of adsorbed gas has been divided into three segments; the first segment is adsorbed entrapped gas which remains trapped in isolated nanopores and hence has no contribution to permeability. The other two segments constitute pressurized gas adsorbed at the surface of the rock which is mainly clay and adsorbed gas within the kerogen which is an organic component. Due to the pressure drop, gas from these two segments diffuses into the pore space causing an increase in the producible gas content or equivalently an enhancement in the permeability. Desorption is mainly a function of reservoir temperature and reservoir pressure while higher temperature and lower pressure conditions favor a higher desorption rate. As pressure drops, pressurized adsorbed gas at the rock (clay) surface is released quickly which is more noticeable in larger pores, as less restraint in flow is present. Desorption contribution to permeability during the earlier time line of the production life is due to the release of the pressurized gas from the rock surface. As the life of the reservoir extends, the desorption of methane coming from the organic component (kerogen) becomes more dominant (Xianggang et al. 2018). The kerogen or organic component within shale constitutes a large proportion of micropores (diameters less than 2 nm) and mesopores (diameters ranging between 2 and 50 nm) based on the pore size standard of the International Union of Pure and Applied Chemistry (IUPAC) (Rouquerol et al. 1994). Due to the desorption occurring from the large fraction of micropores and mesopores, an enhancement in permeability is induced. Table 4 also illustrates that when desorption and slip flow are activated together simultaneously in the model, the enhancement of permeability
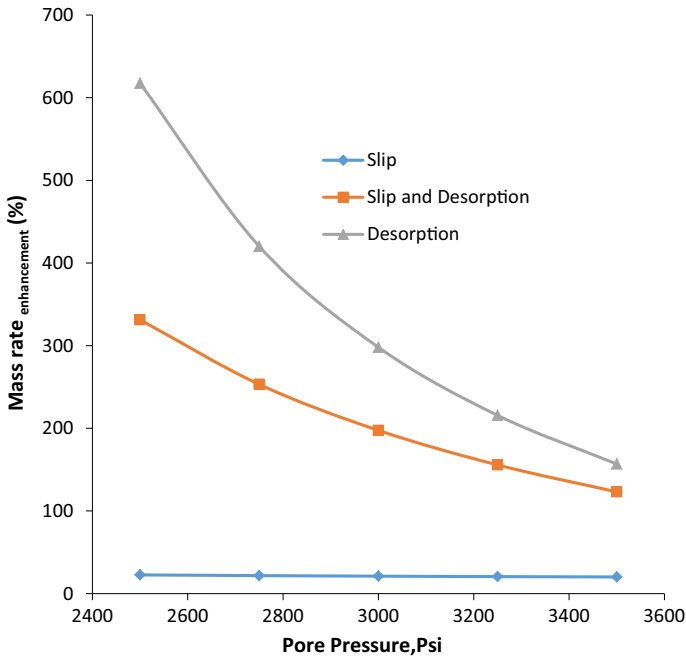
Fig. 12 Mass rate enhancement versus pore pressure

is 23.4% at a high pressure of 3500 Psi and has increased up to 98.5% at a low pressure of 2500 Psi. From these results, it can be observed that the effects of individual slip flow and desorption have not been superposed when they are activated together. In other words, the quantity of net permeability enhancement due to simultaneous effect of slip and desorption is not the summation of the quantities of permeability enhancement due to individual slip and desorption. This is most likely due to the influence of the slippage effect on pressure drop: As the slippage effect is activated, a lower pressure drop is induced within the system, hence limiting the desorption mechanism.

Figure 12 equivalently portrays the contribution of slip flow and desorption mechanism to produced gas mass rate (kg/s) at various pore pressures. Mass rate enhancement is defined below showing the percentage of enhancement of produced mass rate of gas due to slip flow or desorption or also slip together with desorption.

$$\text{Mass rate}_{\text{enhancement}} = \frac{\text{Mass rate}_{\text{with mechanism}} - \text{Mass rate}_{\text{without any mechanism}}}{\text{Mass rate}_{\text{without any mechanism}}} \times 100$$

(20)

In Eq. 20, Mass rate$_{\text{with mechanism}}$ is the mass rate predicted by the model when slip and or desorption is included while Mass rate $_{\text{without any mechanism}}$ is the produced gas mass rate without slip and or desorption.

It can be observed that the inclusion of the desorption term in addition to the slip flow term has clearly resulted in a larger addition to mass rate. This is a result of desorbed methane that is entering the flow stream. The results seem to be shaping a nonlinear relationship between mass flow rate and pore pressure when the effects of desorption and slip are considered. As pressure continues to decrease, the difference in mass rate will be much higher as more
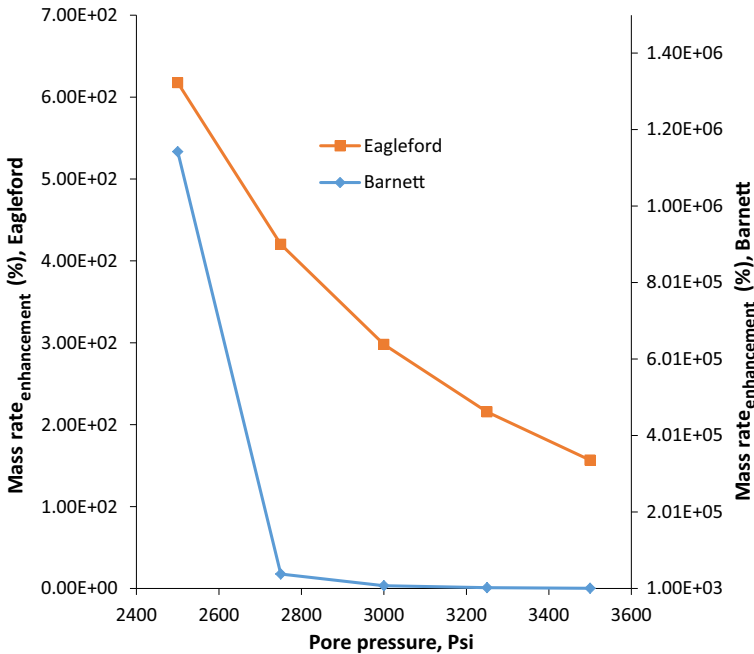
Fig. 13 Mass rate enhancement versus pore pressure due to desorption in Barnett and Eagle Ford samples

adsorbed methane is released. It also shows the importance of considering this mechanism during prediction of gas recovery in shale reservoirs. It has been suggested that the desorption of methane might be partially responsible for the relatively long and flat production tails that have been observed in some shale reservoirs (Valkó and Lee 2010).

Figure 13 compares the contribution of the desorption to produced gas mass rate for Barnett and Eagle Ford shale samples. The results are for gas desorption only without the effect of slip.

From Fig. 13, one can see that the Eagle Ford sample which is characterized by a Langmuir pressure of 4.8 MPa and a Langmuir volume of 12.7 scf/ton portrays a rather subtle increase in the mass flow rate at low pore pressures due to relatively smaller Langmuir volume as compared to the Barnett sample. The Langmuir-type isotherm for Barnett shale sample is characterized by a Langmuir pressure of 4.0 MPa and a Langmuir volume of 74.2 scf/ton stated earlier in Table 3; therefore, the mass flow rate profile is much higher and shows a rapidly increasing rate at low pore pressures. This is due to the larger concentration gradient formed due to the higher volume of adsorbed gas within the Barnett shale system at a fixed pressure in comparison with the Eagle Ford sample at the same pressure.

4 Conclusion

In this paper, a pore scale model was presented to describe gas flow behavior in shale reservoirs including the slip flow and gas desorption mechanism. A pore network model was created using the digitized image of a thin section of a Berea sand stone where it was scaled down to represent the typical pore size within shale reservoirs. Based on the size of the pores in

the network and the pore pressure applied, the Knudsen number ranged between 0.0001 and 0.1, limiting the flow regimes to continuum flow and slip flow. Gas desorption was also considered by fixing a velocity term at the pore's walls derived from Langmuir's isotherm equation. The compressible Stokes flow equation was used in this study. The contribution of slip flow and gas desorption was investigated by calculating the percentage of permeability and mass rate enhancement due to these mechanisms. To consider desorption, the measured isotherm data from the literature for Eagle Ford and Barnett shale samples were used. The results of the model showed that the contribution of desorption was higher than slip in increasing the intrinsic permeability of the system. In other words, desorption could result in a higher permeability enhancement as compared to slip flow. Moreover, it was predicted that the contributions of both slip and desorption are larger at lower pore pressures. Furthermore, it was observed that the desorption contribution was reduced when the slip flow was also activated and the net contribution was not the summation of the individual contribution of each mechanism. That is, the contribution of desorption gas was limited by the slip effect due to the reduced pressure drop. Additionally, a higher mass rate enhancement due to desorption mechanism was predicted for Barnett shale at the same operating conditions due to its larger adsorption isotherm. This study could provide a better understanding of gas desorption mechanism when associated with the slippage effect in recovery of shale gas reservoirs.

References

Ahmadi, M.A., Shadizadeh, S.R.: Experimental investigation of a natural surfactant adsorption on shale-sandstone reservoir rocks: static and dynamic conditions. Fuel **159**, 15–26 (2015)

Batchelor, G.K.: An Introduction to Fluid Dynamics. Cambridge University Press, Cambridge (2000)

Brown, G.P., DiNardo, A., Cheng, G.K., Sherwood, T.K.: The flow of gases in pipes at low pressures. J. Appl. Phys. **17**(10), 802–813 (1946)

Chen, L., Zhang, L., Kang, Q., Viswanathan, H.S., Yao, J., Tao, W.: Nanoscale simulation of shale transport properties using the lattice Boltzmann method: permeability and diffusivity. Sci. Rep. **5**, 8089 (2015)

Cipolla, C.L., Lolon, E., Erdle, J., Tathed, V.: Modeling well performance in shale-gas reservoirs. In: SPE/EAGE Reservoir Characterization and Simulation Conference (2009)

Civan, F.: Effective correlation of apparent gas permeability in tight porous media. Transp. Porous Media **82**(2), 375–384 (2010)

Crain, E.: Crain's Petrophysical Handbook. Spectrum 2000 Mindware Limited, Alberta (2002)

Curtis, J.B.: Fractured shale-gas systems. AAPG Bull. **86**(11), 1921–1938 (2002)

Darabi, H., Ettehad, A., Javadpour, F., Sepehrnoori, K.: Gas flow in ultra-tight shale strata. J. Fluid Mech. **710**, 641–658 (2012)

Etminan, S.R., Javadpour, F., Maini, B.B., Chen, Z.: Measurement of gas storage processes in shale and of the molecular diffusion coefficient in kerogen. Int. J. Coal Geol. **123**, 10–19 (2014)

Fathi, E., Akkutlu, I.Y.: Nonlinear sorption kinetics and surface diffusion effects on gas transport in low-permeability formations. In: SPE Annual Technical Conference and Exhibition 2009. Society of Petroleum Engineers (2009)

Fathi, E., Akkutlu, I.Y.: Lattice Boltzmann method for simulation of shale gas transport in kerogen. SPE J. **18**(01), 27–37 (2012)

Fatt, I.: The network model of porous media. Pet. Trans. AIME **207**, 144–181 (1956)

Fink, R., Krooss, B.M., Gensterblum, Y., Amann-Hildenbrand, A.: Apparent permeability of gas shales—superposition of fluid-dynamic and poro-elastic effects. Fuel **199**, 532–550 (2017)

Freeman, C., Moridis, G., Blasingame, T.: A numerical study of microscale flow behavior in tight gas and shale gas reservoir systems. Transp. Porous Media **90**(1), 253 (2011)

Gad-el-Hak, M.: The fluid mechanics of microdevices—the Freeman scholar lecture. J. Fluids Eng. **121**(1), 5–33 (1999)

Heller, R., Zoback, M.: Adsorption of methane and carbon dioxide on gas shale and pure mineral samples. J. Unconv. Oil Gas Resour. **8**, 14–24 (2014)

Hornbrook, J., Castanier, L., Pettit, P.: Observation of foam/oil interactions in a new, high-resolution micromodel. In: SPE Annual Technical Conference and Exhibition 1991. Society of Petroleum Engineers (1991)

Huang, X., Bandilla, K.W., Celia, M.A.: Multi-physics pore-network modeling of two-phase shale matrix flows. Transp. Porous Media **111**(1), 123–141 (2016)

Javadpour, F.: Nanopores and apparent permeability of gas flow in mudrocks (shales and siltstone). J. Can. Pet. Technol. **48**(08), 16–21 (2009)

Kang, S.M., Fathi, E., Ambrose, R.J., Akkutlu, I.Y., Sigal, R.F.: Carbon dioxide storage capacity of organic-rich shales. SPE J. **16**(04), 842–855 (2011)

Karniadakis, G., Beskok, A., Aluru, N.: Microflows and Nanoflows: Fundamentals and Simulation, vol. 29. Springer, Berlin (2006)

Keller, A.A., Blunt, M.J., Roberts, A.P.V.: Micromodel observation of the role of oil layers in three-phase flow. Transp. Porous Media **26**(3), 277–297 (1997)

Kim, S., Karrila, S.J.: Microhydrodynamics: Principles and Selected Applications. Courier Corporation, North Chelmsford (2013)

Klinkenberg, L.: The permeability of porous media to liquids and gases. In: Drilling and Production Practice, New York, 1 January 1941 (1941)

Langmuir, I.: The constitution and fundamental properties of solids and liquids. Part I. Solids. J. Am. Chem. Soc. **38**(11), 2221–2295 (1916)

Li, J., Yu, T., Liang, X., Zhang, P., Chen, C., Zhang, J.: Insights on the gas permeability change in porous shale. Adv. Geo-Energy Res. **1**, 63–67 (2017)

Lin, D., Wang, J., Yuan, B., Shen, Y.: Review on gas flow and recovery in unconventional porous rocks. Adv. Geo-Energy Res. **1**(1), 39–53 (2017)

Liu, H.-H., Georgi, D., Chen, J.: Correction of source-rock permeability measurements owing to slip flow and Knudsen diffusion: a method and its evaluation. Pet. Sci. **15**(1), 116–125 (2018)

Mehmani, A., Prodanović, M., Javadpour, F.: Multiscale, multiphysics network modeling of shale matrix gas flows. Transp. Porous Media **99**(2), 377–390 (2013)

Moghadam, A.A., Chalaturnyk, R.: Expansion of the Klinkenberg's slippage equation to low permeability porous media. Int. J. Coal Geol. **123**, 2–9 (2014)

Moghaddam, R.N., Foroozesh, J.: Stress dependent capillary dominated flow in matrix around hydraulic fractures in shale reservoirs and its impact on well deliverability. In: SPE Symposium: Production Enhancement and Cost Optimisation 2017. Society of Petroleum Engineers (2017)

Moghaddam, R.N., Jamiolahmady, M.: Slip flow in porous media. Fuel **173**, 298–310 (2016)

Moghaddam, R.N., Aghabozorgi, S., Foroozesh, J.: Numerical simulation of gas production from tight, ultra-tight and shale gas reservoirs: flow regimes and geomechanical effects. In: EUROPEC 2015. Society of Petroleum Engineers (2015)

Moridis, G.J., Blasingame, T.A., Freeman, C.M.: Analysis of mechanisms of flow in fractured tight-gas and shale-gas reservoirs. In: SPE Latin American and Caribbean Petroleum Engineering Conference 2010. Society of Petroleum Engineers (2010)

NIST: NIST chemistry webbook. https://webbook.nist.gov/chemistry/ (2018). Accessed 5 Aug 2018

Pang, Y., Soliman, M.Y., Deng, H., Emadi, H.: Analysis of effective porosity and effective permeability in shale-gas reservoirs with consideration of gas adsorption and stress effects. SPE J. **33**, 1605 (2017)

Rouquerol, J., Avnir, D., Fairbridge, C., Everett, D., Haynes, J., Pernicone, N., Ramsay, J., Sing, K., Unger, K.: Recommendations for the characterization of porous solids (Technical Report). Pure Appl. Chem. **66**(8), 1739–1758 (1994)

Sakhaee-Pour, A., Bryant, S.: Gas permeability of shale. SPE Reserv. Eval. Eng. **15**(04), 401–409 (2012)

Shabro, V., Torres-Verdín, C., Javadpour, F., Sepehrnoori, K.: Finite-difference approximation for fluid-flow simulation and calculation of permeability in porous media. Transp. Porous Media **94**(3), 775–793 (2012)

Sheng, M., Li, G., Huang, Z., Tian, S.: Shale gas transient flow model with effects of surface diffusion. Acta Petrol. Sin. **35**(2), 347–352 (2014)

Sheng, M., Li, G., Huang, Z., Tian, S., Shah, S., Geng, L.: Pore-scale modeling and analysis of surface diffusion effects on shale-gas flow in Kerogen pores. J. Nat. Gas Sci. Eng. **27**, 979–985 (2015)

Singh, H., Javadpour, F.: Nonempirical apparent permeability of shale. In: Unconventional Resources Technology Conference (URTEC) (2013)

Sondergeld, C.H., Newsham, K.E., Comisky, J.T., Rice, M.C., Rai, C.S.: Petrophysical considerations in evaluating and producing shale gas resources. In: SPE Unconventional Gas Conference 2010. Society of Petroleum Engineers (2010)

Song, W., Yao, J., Ma, J., Couples, G., Li, Y.: Assessing relative contributions of transport mechanisms and real gas properties to gas flow in nanoscale organic pores in shales by pore network modelling. Int. J. Heat Mass Transf. **113**, 524–537 (2017)

Strapoc, D., Mastalerz, M., Schimmelmann, A., Drobniak, A., Hasenmueller, N.R.: Geochemical constraints on the origin and volume of gas in the New Albany Shale (Devonian–Mississippian), eastern Illinois Basin. AAPG Bull. **94**(11), 1713–1740 (2010)

Sun, H., Yao, J., Cao, Y.-C., Fan, D.-Y., Zhang, L.: Characterization of gas transport behaviors in shale gas and tight gas reservoirs by digital rock analysis. Int. J. Heat Mass Transf. **104**, 227–239 (2017)

Sutton, R.P., Cox, S.A., Barree, R.D.: Shale gas plays: a performance perspective. In: Tight Gas Completions Conference 2010. Society of Petroleum Engineers (2010)

Valkó, P.P., Lee, W.J.: A better way to forecast production from unconventional gas wells. In: SPE Annual Technical Conference and Exhibition 2010. Society of Petroleum Engineers (2010)

Villazon, M., German, G., Sigal, R.F., Civan, F., Devegowda, D.: Parametric investigation of shale gas production considering nano-scale pore size distribution, formation factor, and non-Darcy flow mechanisms. In: SPE annual technical conference and exhibition 2011. Society of Petroleum Engineers (2011)

Wang, Z., Li, Y., Guo, P., Meng, W.: Analyzing the adaption of different adsorption models for describing the shale gas adsorption law. Chem. Eng. Technol. **39**(10), 1921–1932 (2016)

Wu, K., Li, X., Wang, C., Yu, W., Chen, Z.: Model for surface diffusion of adsorbed gas in nanopores of shale gas reservoirs. Ind. Eng. Chem. Res. **54**(12), 3225–3236 (2015)

Xianggang, D., Zhiming, H., Shusheng, G., Rui, S., Huaxun, L., Chang, J., Lin, W.: Shale high pressure isothermal adsorption curve and the production dynamic experiments of gas well. Petrol. Explor. Dev. **45**(1), 127–135 (2018)

Yang, F., Ning, Z., Zhang, R., Zhao, H., Krooss, B.M.: Investigations on the methane sorption capacity of marine shales from Sichuan Basin, China. Int. J. Coal Geol. **146**, 104–117 (2015)

Zhang, W.-M., Meng, G., Wei, X.-Y., Peng, Z.-K.: Slip flow and heat transfer in microbearings with fractal surface topographies. Int. J. Heat Mass Transf. **55**(23–24), 7223–7233 (2012a)

Zhang, W.-M., Meng, G., Wei, X.: A review on slip models for gas microflows. Microfluid. Nanofluid. **13**(6), 845–882 (2012b)